Flexible and stackable terahertz metamaterials via silver-nanoparticle inkjet printing

K. Kashiwagi, L. Xie, X. Li, T. Kageyama, M. Miura, H. Miyashita, J. Kono, and S.-S. Lee

Citation: AIP Advances **8**, 045104 (2018); doi: 10.1063/1.5006867
View online: https://doi.org/10.1063/1.5006867
View Table of Contents: http://aip.scitation.org/toc/adv/8/4
Published by the American Institute of Physics

Flexible and stackable terahertz metamaterials via silver-nanoparticle inkjet printing

K. Kashiwagi,[1] L. Xie,[2,3] X. Li,[2] T. Kageyama,[1] M. Miura,[1] H. Miyashita,[1] J. Kono,[2,4,5] and S.-S. Lee[1,a]

[1]*Graduate School of Engineering, Tottori University, Tottori 680-8552, Japan*
[2]*Department of Electrical and Computer Engineering, Rice University, Houston, TX 77005, U.S.A.*
[3]*College of Biosystems Engineering and Food Science, Zhejiang University, Hangzhou, Zhejiang 310058, China*
[4]*Department of Physics and Astronomy, Rice University, Houston, TX 77005, U.S.A.*
[5]*Department of Materials Science and NanoEngineering, Rice University, Houston, TX 77005, U.S.A.*

(Received 28 September 2017; accepted 6 March 2018; published online 4 April 2018)

There is presently much interest in tunable, flexible, or reconfigurable metamaterial structures that work in the terahertz frequency range. They can be useful for a range of applications, including spectroscopy, sensing, imaging, and communications. Various methods based on microelectromechanical systems have been used for fabricating terahertz metamaterials, but they typically require high-cost facilities and involve a number of time-consuming and intricate processes. Here, we demonstrate a simple, robust, and cost-effective method for fabricating flexible and stackable multiresonant terahertz metamaterials, using silver nanoparticle inkjet printing. Using this method, we designed and fabricated two arrays of split-ring resonators (SRRs) having different resonant frequencies on separate sheets of paper and then combined the two arrays by stacking. Through terahertz time-domain spectroscopy, we observed resonances at the frequencies expected for the individual SRR arrays as well as at a new frequency due to coupling between the two SRR arrays. © *2018 Author(s). All article content, except where otherwise noted, is licensed under a Creative Commons Attribution (CC BY) license (http://creativecommons.org/licenses/by/4.0/).*
https://doi.org/10.1063/1.5006867

INTRODUCTION

Metamaterials, consisting of periodic arrays of sub-wavelength structures, are becoming increasingly more important in the technologically important terahertz (THz) or far-infrared spectral range. They have been demonstrated to possess unique functionalities that can be employed to manipulate or modulate the amplitude, phase, or polarization of THz waves.[1–6] A variety of methods have been adopted to fabricate THz metamaterials. Among them, methods based on microelectromechanical systems (MEMS) are considered promising for making reconfigurable THz metamaterials on a flexible substrate. However, high-cost facilities are needed for fabricating metamaterials using MEMS, and a number of time-consuming and intricate processes are involved in MEMS-based fabrication procedures.

Here, we propose and demonstrate a simple, robust, and cost-effective method for fabricating multiresonant THz metamaterials on flexible substrates using an ordinary printer with conductive ink containing silver (Ag) nanoparticles. A similar method was recently used for fabricating a THz plasmonic structure, and its feasibility was successfully demonstrated.[7,8] A similar method was recently used for fabricating a THz plasmonic structure, and its feasibility was successfully demonstrated.[9] In this report, specifically, we fabricated a two-dimensional array of split-ring

[a]Corresponding author: sslee@eecs.tottori-u.ac.jp

 © Author(s) 2018

resonators (SRRs) on a sheet of paper. Furthermore, we stacked two sheets of paper having two-dimensional arrays of SRRs with different resonance frequencies. The two arrays of SRRs were stacked using a screen printing technique, while polyimide was used as the adhesive for stacking, making this a low-cost fabrication method to obtain multilayers of metamaterials. The stacking of two layers also created a third resonance frequency, resulting from the coupling of the two arrays of SRRs.

SIMULATION

We performed finite element method (FEM) simulations to design a metamaterial structure made of silver (Ag) nanoparticles with a desired resonance frequency, utilizing a FEM software package of COMSOL Multiphysics. Figure 1 schematically shows the model used, which consists of upper and lower printed SRR arrays, paper sheets as substrates, and a polyimide layer as adhesive to combine the two sheets of paper. One SRR for each layer is shown in Fig. 1, but periodic boundary conditions were employed in the simulation to represent the periodicity of the SRR arrays. The upper SRRs were arrayed with a 400 μm gap between SRRs. Each lower SRR was placed to have the same optical axis of each corresponding upper SRR. In simulating transmission spectra for these structures, we used air as the reference. The dimensions of the designed SRRs were as follows: The one side length (l), the width (w), and the capacitive gap (g) of the upper SRRs, as shown in Fig. 1, were 400 μm, 50 μm, and 100 μm, respectively. On the other hand, in the lower SRRs, l was 300 μm, while g and w were the same as those of the upper SRRs. The thickness of SRRs was about 10 μm, determined by the inkjet print-head ability. The permittivity and thickness of the substrate paper were considered to be 2.24+0.3i and 235 μm, respectively. Furthermore, the permittivity and thickness of the polyimide adhesive layer were assumed to be 2.4 and 22 μm, respectively.

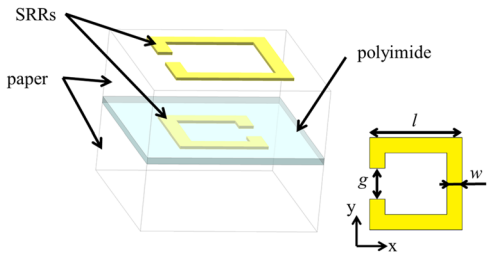

FIG. 1. Schematic view of a finite element method simulation model of our SRRs. Two kinds of SRRs with different dimensions were used. The main design parameters of each of the SRR arrays are the length (l), width (w), gap (g), and the distance between adjacent SRRs within each array.

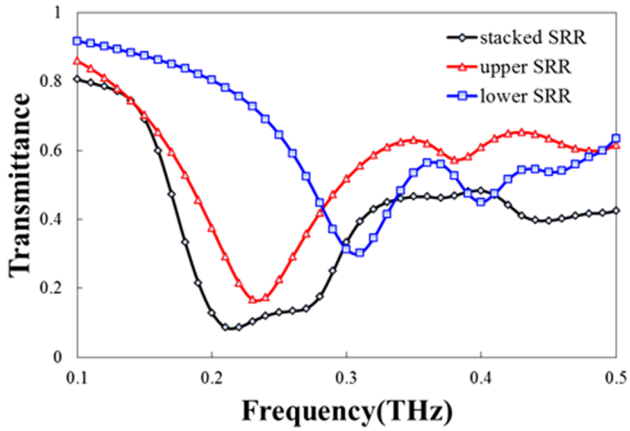

FIG. 2. THz transmission spectra for the individual and stacked SRR arrays, simulated through the finite element method.

The FEM simulation results are shown in Fig. 2. We obtained resonance frequencies of 0.23 THz and 0.31 THz for individual upper and lower SRR arrays, respectively. After stacking, resonance frequencies were confirmed to be 0.21 THz, 0.27 THz, and 0.37 THz. They resulted from the resonances of the upper and lower SRRs, and the effect of stacking. The slight red shift observed for each layer is due to the additional parallel parasitic capacitances between SRRs. The parasitic capacitance effect on the lower SRRs through the dielectric polyimide layer is larger than that on the upper SRRs due to the smaller physical distance between the polyimide layer and the SRR arrays. The dip at 0.37 THz represents the newly generated resonance frequency due to stacking. It is caused from the additional serial parasitic capacitance between the upper and lower SRR arrays through the dielectric polyimide layer.

FABRICATION

We fabricated stacked SRR arrays based on the simulation results by using Ag nanoparticle inkjet printing. We used an ordinary inkjet printer (DCP-J740N, Brother Industries, Ltd., Nagoya, Japan) with ink containing Ag nanoparticles, which was developed by AgIC Inc.[10] for the purpose of conductive line drawing on a flexible substrate, such as paper and plastics. This ink is useful as a low-cost and high-speed circuit fabrication tool on flexible substrates.[11] It does not require any additional treatment, such as baking, after printing, and it takes only a few seconds to dry after printing. The basic characteristics of the Ag nanoparticle ink used are summarized in Table I.

Before fabricating stacked SRR arrays, we investigated the performance of the print head. In order to have resonance frequencies in the THz range, we have to be able to print fine patterns with 50 μm wide conductive lines having a 100 μm wide gap. Printing pattern data was prepared by CAD software. We prepared six kinds of SRRs, whose line widths were 50 μm, 100 μm, and 150 μm, with two capacitive gaps of 50 μm and 100 μm, respectively. We printed 48 SRRs per 6 different SRR patterns, and examined the printed patterns with a microscope. By examination through naked eyes, we counted the number of defective SRRs, i.e., those SRRs that have a broken conductive line or an ill-shaped capacitive gap. The counted numbers for six different SRR patterns are summarized in Table II as error rates of printing. The overall pattern error rate was 14.6% for our designed SRR pattern, which is acceptable for the current purposes. However, we also concluded that it is not possible to achieve SRR patterns having a narrower gap of 50 μm for any examined width. Moreover, in the case of 100 μm capacitive gap, the larger the pattern width became, the more reliable the

TABLE I. Characteristics of Ag nanoparticle ink.[10]

Composition	-Silver (15% wt) -Water -Ethylene glycol -Ethanol
Sheet resistance	0.2 [Ω/sq]
Viscosity	2 - 3 [mPa•s]
Surface tension	30 - 35 [mN/m]

TABLE II. Pattern error rates of printed patterns with Ag nanoparticle ink for six different SRR patterns.

Width [μm]	gap [μm]	Error rate [%]
50	50	62.5
	100	14.6
100	50	60.4
	100	2.1
150	50	66.7
	100	2.1

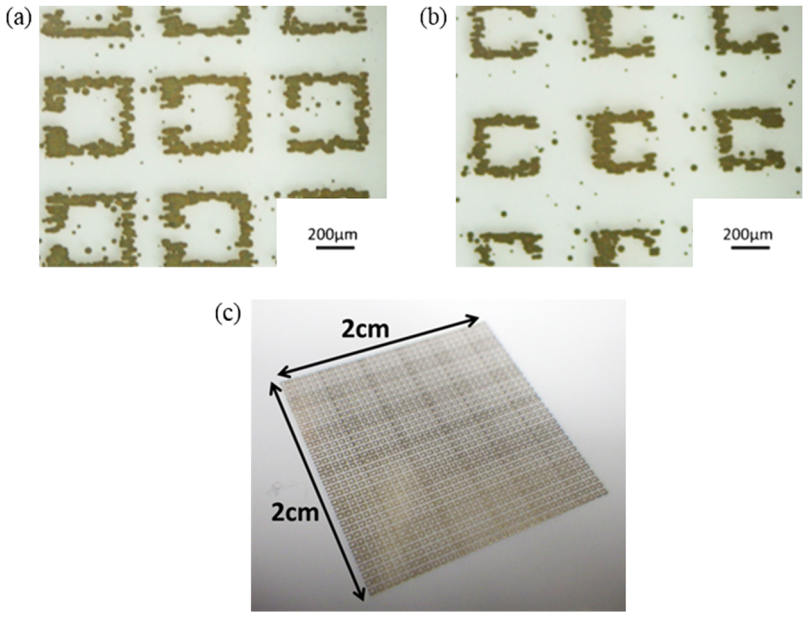

FIG. 3. Printed SRRs using Ag nanoparticle ink: (a) upper SRRs, (b) lower SRRs, and (c) overall view of the printed SRRs.

obtained pattern became. This means that Ag nanoparticle inkjet printing on a flexible substrate is also applicable to microwaves. The spatial resolution of inkjet printing can be improved in the future by reducing the size of the inkjet head nozzle.

Printed SRR arrays are shown in Fig. 3. The upper and lower SRR arrays were printed individually on a 2 cm^2 and 235 μm thick sheet of inkjet paper. The dimensions of the SRR arrays were determined based on our simulation results to have resonance frequencies in the THz range. Note that in Figs. 3(a) and (b) splattered droplets of Ag nanoparticle ink are seen between SRR patterns, but their influence on the *LC* values of the SRRs is negligible. During printing, we also placed cross-shaped alignment marks at the four corners of the paper to align the optical axes of the upper and lower SRR arrays.

After Ag nanoparticle inkjet printing, we stacked the two SRR arrays by using a low-cost screen-printing technique. As an adhesive layer between the two sheets of paper, we used a polyimide film. In Fig. 4, a schematic diagram of the stacking process is illustrated. First, we located the printed lower SRR array beneath the screen-printing mask frame [Fig. 4(a)]. The screen-printing mask within the frame was made of woven stainless steel fibers. In the mask, the area not necessary for deposition was blocked by resist. Next, we poured polyimide onto the screen-printing mask [Fig. 4(b)], and then, the polyimide was pulled and extruded with a silicone rubber squeegee [Fig. 4(c)]. Consequently, we obtained a ~22 μm thick transferred polyimide film layer on the lower SRR array [Fig. 4(d)].

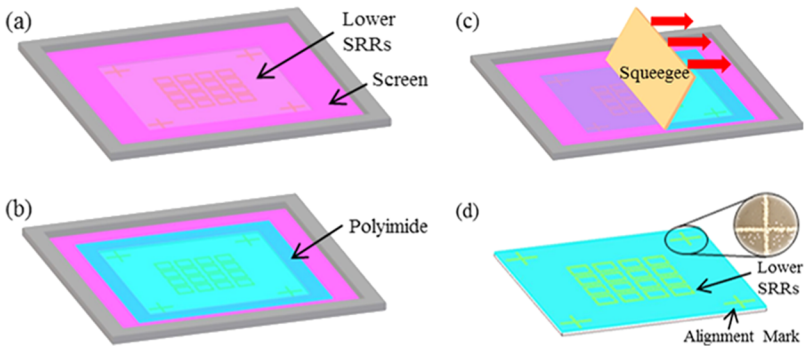

FIG. 4. Stacking process of two SRR arrays by using a screen-printing technique.

In Fig. 4(d), alignment marks at the four corners are indicated. For the alignment process, we pre-arranged needles at the same intervals as the alignment marks. We stung the center of the alignment marks on the lower substrate with the polyimide layer to the needles. Finally, we achieved stacked SRR arrays by overlaying the upper substrate onto the lower substrate with the polyimide layer. After stacking, we performed thermal treatment to harden the liquid-like polyimide layer. To avoid the deterioration of Ag nanoparticle ink and the deformation of paper, the thermal treatment was performed at 80°C for 10 hours. In total, we fabricated three upper SRR arrays, three lower SRR arrays, and three stacked SRR arrays.

MEASUREMENT RESULTS AND DISCUSSION

In order to characterize our stacked SRR arrays, we measured THz transmission through the nine samples by THz time-domain spectroscopy (THz-TDS): three upper SRR array samples, three lower SRR array samples, and three stacked SRR array samples. Each of the last three samples consisted of an upper SRR array and a lower SRR array, which were fabricated separately and measured individually. The THz wave was normal incident onto the SRR array plane in the frequency range of 0.1–0.5 THz. We measured the transmittance for both *x*- and *y*-polarized THz waves. Moreover, we measured individual upper and lower SRR arrays as well as stacked SRRs arrays that were fabricated by the same fabrication process.

The measured transmittance spectra for the upper and lower SRR arrays for *x*- and *y*-polarized incident waves are shown in Fig. 5 and Fig. 6, respectively. The simulation results are also shown for comparison, and they showed reasonable agreement with the measurement results. To obtain better agreement, the physical parameters in the simulations and the uniformity in the fabrication process have to be refined.

In Fig. 5(a), a resonance at 0.21 THz is observed for an *x*-polarized incident wave. On the other hand, two resonance frequencies of 0.28 THz and 0.38 THz exist for a *y*-polarized incident wave, as shown in Fig. 5(b). Though the resonance frequency of 0.38 THz is slightly red-shifted from

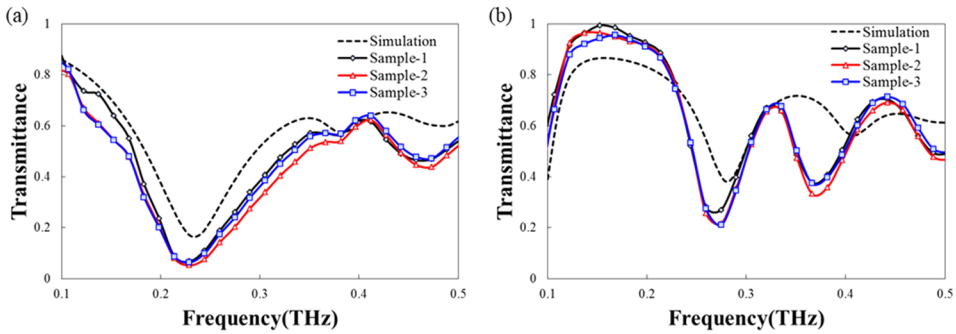

FIG. 5. Experimentally measured transmittance spectra for the upper SRR array for (a) *x*- and (b) *y*-polarized incident waves.

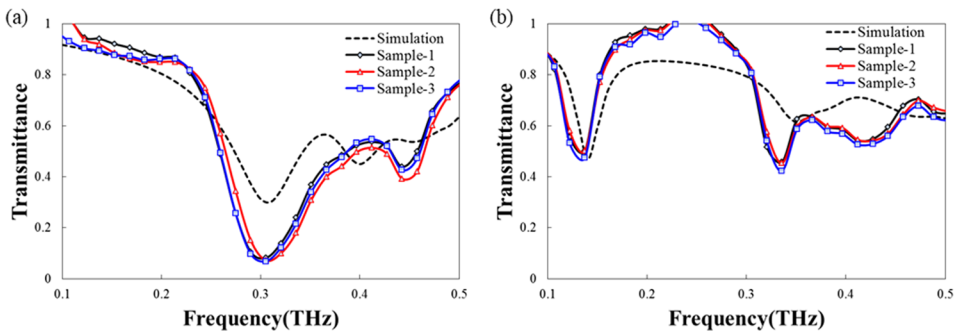

FIG. 6. Transmittances of the lower SRR array for (a) *x*- and (b) *y*-polarized incident waves.

the simulation value (0.41 THz), the simulation results agree well with the measurement results. Furthermore, essentially the same spectra were observed for the three samples, suggesting that the reproducibility and uniformity of the SRR array printing process.

Similarly, in the case of the lower SRR array sample, we also obtained resonance frequencies of 0.3 THz, and 0.14 THz and 0.34 THz for *x*-, and *y*-polarized incident waves, respectively. Moreover, rough agreement between simulation and measurement results as well as sample-to-sample reproducibility were confirmed.

Measured transmittance spectra for the stacked SRR arrays for *x*- and *y*-polarized incident waves are shown in Fig. 7. As shown in Fig. 7(a), we observed dips at 0.2–0.3 THz and 0.37 THz for *x*-polarization. In the simulation, two dips at 0.21 THz and 0.27 THz corresponding to resonance frequencies of the upper and lower SRR arrays, respectively, were obtained in the 0.2–0.3 THz range. However, these two resonances were not distinguishable experimentally. Although a peak between the two resonance frequencies of 0.21 THz and 0.27 THz was broadened, we believe that two resonance frequencies exist because the broadened dip actually ranges between 0.21 THz and 0.27 THz, as shown in Fig. 7(a). For the same reason, we consider our simulation results of the stacked SRR arrays to agree with the measurement results reasonably. Notably, differences of the measurement results for *x*-polarized incident wave were small, which means that there was no large error in printing the conductive lines along the *x* axis (see, Fig. 1).

On the other hand, in the case of *y*-polarized incident waves, we also obtained multiple resonances at frequencies of 0.11 THz, 0.27 THz, and 0.39 THz, as shown in Fig. 7(b). Specifically, Sample No. 3 showed spectra very close to the simulated results. The overall behaviors of Samples 1 and 2 were also similar to the simulated result, although the transmittance values were comparably high. In Samples 1 and 2, there are possibilities of high error rates in printing conductive lines along the *y* axis in the SRRs (see, Fig. 1). Note that the upper and lower SRR arrays used in the fabrication of stacked SRR arrays were printed separately; in other words, they were different arrays used in the measurements for the study of individual arrays.

In order to investigate the possible influence of misalignment between the upper and lower SRR arrays on the resonance frequencies of the stacked SRR array, we performed additional simulations. We intentionally shifted the two SRR arrays in the stacking process by +50 μm and +100 μm along the *x* and *y* axis, respectively. The obtained simulation results are shown in Fig. 8, clearing demonstrating the influence of misalignment. Figure 8(a) shows that for an *x*-polarized incident wave the resonances in the 0.2–0.3 THz range is broadened. In addition, the transmittance value at 0.37 THz is seen to depend on the amount of misalignment along the *x*-direction. For a *y*-polarized incident wave, the resonance frequency of 0.39 THz red-shifts by an amount proportional to the misalignment along the *x*-direction. As a result, we conclude that the alignment accuracy between the upper and lower SRR arrays in the stacked SRR array is one of important fabrication parameters to obtain precise resonance frequencies of stacked SRR arrays. To achieve more precise resonance frequencies, we have to develop a more accurate alignment method. For instance, punching using laser micromachining at the center of the alignment mark or the development of a jig for better overlapping would provide

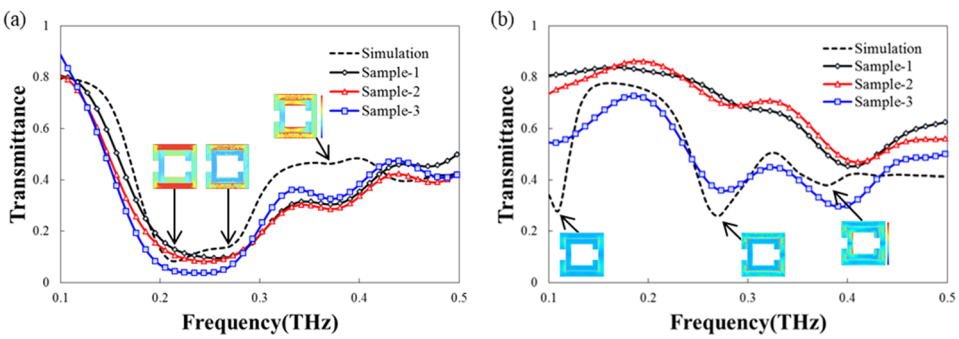

FIG. 7. Transmittances of the stacked SRR arrays for (a) *x*- and (b) *y*-polarized incident waves. Insets in (a) and (b) represent simulated TE-modes on the top surfaces of SRRs at the resonance frequencies.

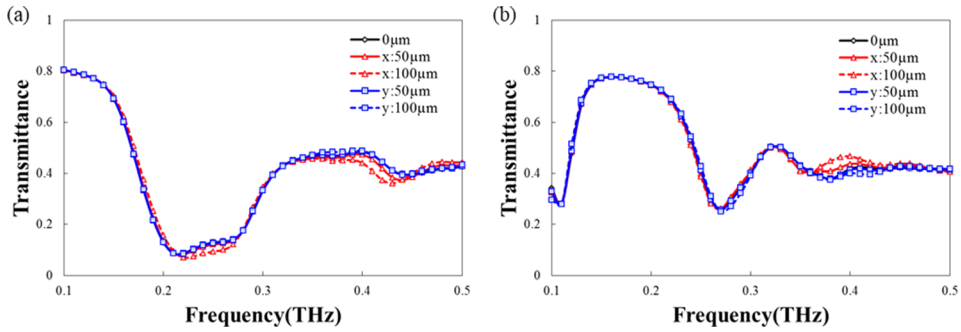

FIG. 8. Simulation results when the two SRR arrays are misaligned by +50 μm and +100 μm from the center along the *x* and *y* axes, respectively, for (a) *x*- and (b) *y*-polarized incident waves.

better results. Moreover, to achieve sharper dips, the Q values of the upper and lower SRRs at the resonance frequencies should be improved, since we observed not completely separated resonance mode especially at 0.27 THz through the simulated TE-modes on each SRR top surface as shown in the Fig. 7(a) insets. In other words, as shown in the Fig. 7(a) insets, although we confirmed the dominant resonance modes through the simulated TE-modes on the top surfaces of the upper and lower SRRs as well as the coupled resonance mode of the stacked SRRs at each corresponding resonant frequency, the absorbance of the upper SRR at 0.27 THz still exists.

CONCLUSION

In conclusion, we demonstrated a multiresonant SRR array with a stacked structure fabricated on sheets of paper by Ag nanoparticles inkjet printing. We used a screen-printing technique to insert a polyimide layer as adhesive in fabricating the stacked SRR arrays. Fabricated stacked SRR arrays were characterized by THz-TDS. Through transmittance measurements, we successfully confirmed the multiple resonances for *x*-polarized incident waves at frequencies of 0.21 THz, 0.27 THz, and 0.37 THz, which showed reasonable agreement with our simulation results. Our fabrication method is considered as a cost-effective and rapid prototyping tool to achieve a large area multiresonant THz metamaterials on a flexible substrate.

ACKNOWLEDGMENTS

We thank the PI R&D Co., Ltd. Yokohama, Japan and AgIC Inc., Tokyo, Japan for the provision of their adhesive polyimide resin and Ag nanoparticles ink, respectively.

[1] P.–Y. Chen and A. Alu, "Atomically thin surface cloak using graphene monolayers," ACS Nano **5**, 5855–5863 (2011).
[2] F. Zhou, Y. Bao, W. Cao, C. T. Stuart, J. Gu, W. Zhang, and C. Sun, "Hiding a realistic object using a broadband terahertz invisibility cloak," Scientific Reports **1** (2011).
[3] D. Liang, J. Gu, J. Han, Y. Yang, S. Zhang, and W. Zhang, "Robust large dimension terahertz cloaking," Advanced Materials **24**, 916–921 (2012).
[4] N. R. Han, Z. C. Chen, C. S. Lim, B. Ng, and M. H. Hong, "Broadband multi-layer terahertz metamaterials fabrication and characterization on flexible substrates," Optics Express **19**, 6990–6998 (2011).
[5] H. Zhou, F. Ding, Y. Jin, and S. He, "Terahertz metamaterial modulators based on absorption," Progress in Electromag. Res. **119**, 449–460 (2011).
[6] H.-T. Chen, "Interference theory of metamaterial perfect absorbers," Optics Express **20**, 7165–7172 (2012).
[7] K. Takano, T. Kawabata, C.-F. Hsieh, K. Akiyama, F. Miyamaru, Y. Abe, Y. Tokuda, R.-P. Pan, C.-L. Pan, and M. Hangyo, "Fabrication of terahertz planar metamaterials using a super-fine ink-jet printer," Appl. Phys. Express **3**, 016701 (2010).
[8] K. Murata and K. Kasuda, Super Ink-Jet Printer Technology and Its Properties. *Convertech & e-Print (July/Aug)* 2011, 74–78.
[9] B. Gupta, S. Pandey, S. Guruswamy, and A. Nahata, "Terahertz plasmonic structures based on spatially varying conductivities," Advanced Optical Materials **2**, 565–571 (2014).
[10] For more detailed information, see https://agic.cc/en.
[11] Y. Kawahara, S. Hodges, B. S. Cook, C. Zhang, and G. D. Abowd, "Instant inkjet circuits: Lab-based inkjet printing to support rapid prototyping of UbiComp devices," *Proc. of the 2013 ACM International Joint Conference on Pervasive and Ubiquitous Computing* 2013, 363–372.